Catalytic, NonCatalytic, and Inhibitory Phenomena: Kinetic Analysis of (4-Hydroxyphenyl)pyruvate Dioxygenase from *Arabidopsis thaliana*†

Vincent M. Purpero and Graham R. Moran*

Department of Chemistry and Biochemistry, University of Wisconsin-Milwaukee, 3210 N. Cramer Street, Milwaukee, Wisconsin 53211-3029

Received November 24, 2005; Revised Manuscript Received February 25, 2006

ABSTRACT: (4-Hydroxyphenyl)pyruvate dioxygenase (HPPD) incorporates both atoms of molecular oxygen into 4-hydroxyphenylpyruvate (HPP) to form homogentisate (HG). This reaction has direct relevance in both medicine and agriculture. In humans, the specific inhibition of HPPD alleviates the symptoms of diseases that arise from tyrosine catabolism defects. However, in plants, the inhibition of HPPD bleaches, stunts, and ultimately kills the organism. The reason for this is that in mammalian metabolism the product HG does not feed into other pathways, whereas in plants it is the precursor for the redox active portion of tocopherols and plastoquinones. There are a number of commercially available herbicides that directly target the inhibition of the HPPD reaction. Plant HPPD however is largely uncharacterized in terms of its catalysis and inhibition reactions. In this study, we examine the catalysis and inhibition of HPPD from *Arabidopsis thaliana* (AtHPPD). We have expressed AtHPPD and purified the enzyme to high specific activity. This form of HPPD accumulates two transient species in single turnover reactions with the native substrate HPP. These transients appear to be equivalent to intermediates I and III observed in the enzyme from *Streptomyces* (Johnson-Winters et al. (2005), *Biochemistry*, 44, 7189−7199). The first intermediate is a relatively strongly absorbing species with maxima at 380 and 490 nm. This species decays to a second intermediate that is fluorescent and has been assigned as the complex of the enzyme with the product, HG. The decay of this intermediate is rate-determining in multiple turnover reactions. The reaction of the enzyme with the analogue of the substrate, phenylpyruvate (PPA), is noncatalytic. A single turnover reaction is observed with this ligand that renders the enzyme oxidized to the ferric form, consumes a stoichiometric amount of dioxygen, and yields 66% phenylacetate as a product. Additional absorbance features at 365 and 670 nm accumulate during inactivation and give the inactivated enzyme a green color but has the same molecular mass as the active enzyme as determined by mass spectrometry.

Earlier studies with a bacterial form of HPPD[1] indicated that triketone inhibitors associate slowly in multiple steps to form an irreversible complex with the active site ferrous ion (Kavana, M., and Moran, G. R. (2003) *Biochemistry*, 42, 10238−10245). Inhibition of AtHPPD was observed with NTBC, the drug used to treat diseases of tyrosine catabolism, and Mesotrione, the primary HPPD inhibitor sold as a herbicide. These data indicate that the mechanism of association of both molecules is remarkably similar. Moreover, the kinetic mechanism of association would appear to be equivalent to that observed in the bacterial form of the enzyme, where a three step binding mechanism results in the formation of an irreversible complex of the inhibitor with the ferrous holoenzyme.

The reaction catalyzed by 4-hydroxyphenylpyruvate dioxygenase (HPPD) is the first committed step of tyrosine catabolism and is common to virtually all organisms that respirate aerobically. HPPD is one of a large family of Fe(II)-dependent oxygenases that reduce dioxygen to bring about the decarboxylation of an α-keto acid (generally α-ketoglutarate (AKG)) to drive hydroxylation or oxidation of a third substrate that is enzyme specific (*1*). HPPD is one of three known exceptions in this family of enzymes that have an α-keto acid as part of a substrate that is ultimately hydroxylated and thus do not use AKG. The structure and substrate-liganding interactions of HPPD are more similar to those of the extradiol-type dioxygenase enzymes (*2*, *3*). It is therefore assumed that HPPD evolution diverged in terms of structure from an extradiol dioxygenase progenitor and converged in terms of mechanism to bind an α-keto acid moiety to instigate the reaction with dioxygen (*4*, *5*). The reaction catalyzed by HPPD is particularly interesting because the hydroxylation reaction displaces an aceto-subsituent in an NIH-shift to the adjacent carbon on the aromatic ring (Scheme 1) (*6*). Our laboratory has been interested in defining the reaction coordinate of HPPD to establish how the transformation from HPP to homogentisate (HG) is catalyzed. Using HPPD from *Streptomyces*, we have

† This research was supported by the National Institutes of Health Grant DK59551.

* To whom correspondence should be addressed. Tel: (414) 229 5031. Fax: (414) 229 5530. E-mail: moran@uwm.edu.

[1] Abreviations: NTBC, 2-(2-nitro-4-(trifluoromethyl)benzoyl)-1,3-cyclohexanedione; HEPES, (*N*-(2-hydroxyethyl)piperizine-*N*′-(2-ethane sulfonic acid)); HPPD, (4-hydroxyphenyl)pyruvate dioxygenase; HPP, (4-hydroxyphenyl)pyruvate; HG, homogentisate (2,5-dihydroxyphenylacetic acid); PPA, phenylpyruvate; PA, phenylacetate, α-ketoglutarate; AKG.; EPR, electron paramagnetic resonance; βME, β-mercaptoethanol; 2HPA, 2-hydroxyphenylacetic acid.

10.1021/bi052409c CCC: $33.50
Published on Web 04/25/2006

Scheme 1

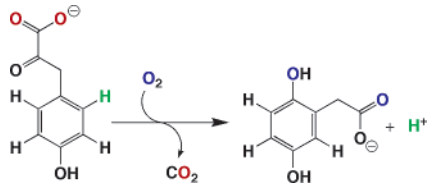

spectrophotmetrically observed, the pre-steady-state accumulation of three intermediates in the time frame of a single turnover (*7*). Evidence suggests that the second intermediate is either an epoxide or dienone tautomer of the product, and the third intermediate is the homogentisate complex. The identity of the first and most strongly absorbing intermediate is unknown.

The results presented here indicate that AtHPPD shares two intermediates with HPPD from *Streptomyces* (SaHPPD). Moreover, the *Streptomyces* enzymes shows no reactivity with phenylpyruvic acid (PPA) (*4*), whereas AtHPPD will undergo a single abortive turnover with this molecule that renders the enzyme inactive and does not yield the predicted 2-hydroxyphenylacetic acid (2HPA) product. These observations are at odds with the generally accepted notion that both HPP and PPA are substrates for HPPD (*8*−*18*).

The activity of HPPD in plants has special significance in that HG is the branch point to a biosynthetic pathway that forms tocopherols and plastoquinones. Tocopherols are required for growth and stress responses. Plastoquinone shuttles electrons from photosystem II to photosystem I in the chloroplast membrane and also serves as the cofactor for phytoene desaturase, the enzyme that catalyzes the committed step of carotenoid biosynthesis (*19*). Thus, the inhibition of HPPD leads to stunting, bleaching, and the eventual death of plants. In the late 1960s, Hellyer observed the allelopathic capacity of a number of myrtaceous Australian plants. The active inhibitory agent from these plants was found to be leptospermone, a specific inhibitor of HPPD (*20*). Other natural HPPD inhibitors such as usnic acid from lichens have also been discovered (*21*). The common structural motif of these molecules is a 1,3-diketone, emerging from a multi-ring structure (Chart 1). Since the early 1980s, agrochemical interests have attempted to develop mimics of these natural inhibitors such that they could be used as herbicides (*22*−*24*). One of the earliest developed was 2-(2-nitro-4-(trifluoromethyl)benzoyl)-1,3-cyclohexanedione (NTBC) (*25*). Although this molecule had potent activity in plants, it persisted in mammalian metabolism, and this prevented it from being adopted for herbicidal use (*26*). This persistence later lead to the use of NTBC in the treatment of the lethal tyrosine catabolism defect, type 1 tyrosinemia (*27*), and, subsequently, in a second debilitating defect, alkaptonuria (*28*−*31*). Variations on the NTBC structure have produced molecules that exhibit much reduced half-lives in mammalian metabolism (*23*, *32*, *33*). One such molecule, Mesotrione, is currently marketed as a Callisto herbicide by Syngenta.

The interaction of NTBC with a bacterial form of HPPD was recently demonstrated. The inhibitor was shown to associate in three steps with the HPPD active site metal ferrous iron to form an irreversible complex that completely suppressed the dioxygen reactivity of the metal (*34*). This latter observation lead to crystallization and structural

Chart 1: Representative HPPD Inhibitors

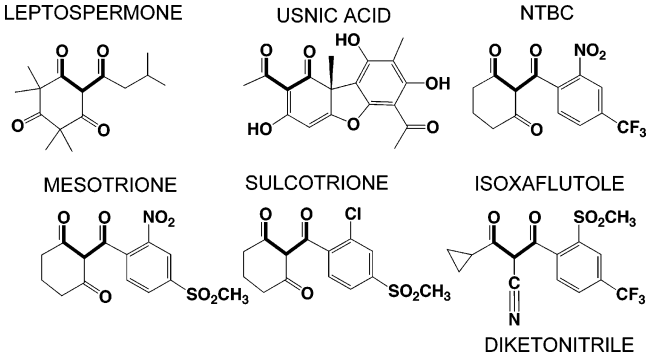

elucidation of the HPPD·Fe(II)·NTBC complex (*35*). These studies settled much of the conjecture that had persisted in regard to the inhibition of HPPD by such molecules. However, the one deficiency of these investigations was that all observations were made with a form of HPPD to which such molecules are not normally applicable, naturally, therapeutically, or commercially. As such, we have expressed and purified HPPD from *Arabidopsis thaliana* (AtHPPD) to establish if the observations made with NTBC and bacterial HPPD hold more generally.

MATERIALS AND METHODS

Materials. NTBC was a gift from Syngenta via Orphan Pharmaceuticals, and Mesotrione was obtained as a suspension in Syngenta's Callisto herbicide. HEPES buffer, Fe(II) sulfate heptahydrate, trichloroacetic acid, βME, HPP, and 2-hydroxyphenylacetic acid (2HPA) were purchased from ACROS. Citrate, streptomycin sulfate, enzyme grade ammonium sulfate, and LB broth were from Fisher Scientific. PPA, sodium hydroxide, HPLC grade acetonitrile, and HPLC-grade methanol were from Sigma-Aldrich Chemical Co. Phenyl acetic acid was obtained from Alfa Aesar. The BL21 DE3 *E. coli* cells were from Invitrogen. Agarose and isopropyl-β-thiogalactopyranoside (IPTG) were acquired from ICN Biomedicals. An analytical reverse-phase phenyl column (4.6 × 250 mm) was obtained from Phenomenex. Biomax 10 kDa MWCO centrifugal filters were purchased from Amicon. MacroPrep High Q Support column packing was purchased from Bio-Rad. Sephacryl S-200 size exclusion column packing was from GE Biosciences.

Expression and Purification of AtHPPD. The plasmid pET-HPP was prepared from the pET15b expression vector (*36*) and contained the HPPD gene from *Arabidopsis thaliana*. This construct was a gift from the laboratory of Dr. Dean Della Penna at Michigan State University (*37*). The plasmid was transformed into chemically competent Top Ten BL21 DE3 *E. coli* cells and stored at −80 °C in 1 mL of Luria−Bertani broth (LB) aliquots containing 20% glycerol. Upon thawing, the cells were spread on LB/ampicillin agar plates (two per liter of culture) and grown for 10−15 h at 37 °C. The Luria−Bertani broth (10 mL) was used to resuspend the cells from the plates. This suspension was then used to inoculate the LB broth containing 100 μg/mL of ampicillin. The cells were then grown for 12 h without induction by IPTG and harvested by centrifugation at 4665*g* for 30 min using an Sorval RC-3C centrifuge.

The purification protocol involved significant modifications of the procedure of Yang et al. (*38*). Cell pellets were

resuspended in 20 mM HEPES buffer at pH 7.0, 15 mL/L of culture and sonicated on ice using a Branson Sonifier 450 fitted with a blunt tungsten tip for 2 × 6 min at 45 W, ensuring that the temperature of the sonicate did not increase beyond 10 °C. All subsequent steps of purification were performed at 4 °C. The sonication slurry was centrifuged at 33 000 *g* for 30 min, and the supernatant was brought to 1.75% (w/v) streptomycin sulfate. This solution was then centrifuged at 19 000 *g* for 10 min, and the supernatant was brought to 40% ammonium sulfate saturation. This mixture was then centrifuged at 19 000 *g* for 10 min, and the supernatant was then brought to 50% ammonium sulfate saturation and centrifuged again at 19 000 *g* for 10 min. The pellet from this step was then resuspended in 20 mM HEPES at pH 7.0 (~100 mL/L culture) and loaded onto a Q sepharose anion exchange column at a rate of 1 mL/min. The protein was eluted with a linear gradient of sodium chloride (0−150 mM) over 560 min at a rate of 1 mL/min. The column fractions (5 mL each) that showed activity were pooled (~80 mL), and the sample was then concentrated at 4000*g* using an Amicon Biomax 10 kDa MWCO filter (15 mL) to approximately 3 mL. This protein was then loaded onto a Sephacryl S-200 size exclusion column (2.5 × 100 cm) and eluted at 1 mL/min in 20 mM HEPES at pH 7.0. Active fractions were pooled and stored at −80 °C.

Chemical Preparation and Extinction Coefficients. The extinction coefficient of AtHPPD was calculated to be 29 630 M^{-1} cm^{-1} at 280 nm by the method of Pace (*39*). The molar extinction coefficient of NTBC was 20 550 M^{-1} cm^{-1} at 257 nm as previously reported (*34*). To obtain pure Mesotrione, the Callisto herbicide suspension slurry was filtered onto Whatman grade 41 filter paper and briefly washed with water to obtain the solid fraction. The purity of the sample was assessed by NMR. Mesotrione has an extinction coefficient of 26 500 M^{-1} cm^{-1} at 256 nm, which was determined using the NMR internal standard method of Johnson-Winters et al. (*7*). PPA was purchased with 98% purity, and further purified using HPLC. A Phenomenex semiprep phenyl column (21.2 × 250 mm) isocratically run at 5 mL/min using 20 mM citrate at pH 3.5 allowed for PPA to be resolved from impurities. The PPA was collected and dried by lyophilization. The PPA and citrate mixture was dissolved in water and injected again onto the phenyl semiprep column and desalted by using 18 MΩ deionized water as the running buffer. The PPA sample was collected and lyophilized resulting in a white crystalline powder that was stored at −80 °C. To quantify, the PPA stocks were allowed to equilibrate to the diol form in 100 mM TCA (pH 1.5) for 1 h. The absorbance spectrum of the resulting peak had a λ_{max} at 290 nm and gave an extinction coefficient of 2 130 M^{-1} cm^{-1}, which was also determined using the internal NMR standard method. All other extinction coefficients were as previously reported (*4*).

Activity Assays for HPPD. The activity of AtHPPD was polarographically measured with a Hansatech Oxygraph oxygen electrode. Standard activity assays included 0.5 μM of enzyme, 500 μM βME, Fe(II) stoichiometric with enzyme, and 400 μM HPP in 20 mM HEPES at pH 7.0 with atmospheric oxygen (~250 μM). Reactions were initiated with HPP, and rates were measured from the first 20 to 40 s of turnover. Both dioxygen and HPP were varied to determine the steady-state kinetic constants of AtHPPD at 4 °C for direct comparison to pre-steady-state data measured at the same temperature. These data were fit globally using Nonlin (Rubelko Software) to eq 1, which describes an ordered or random bireactant system.

$$v = \frac{(V_{max}[HPP][O_2])}{(K_{i\,HPP}K_{O2}) + (K_{HPP}[O_2]) + (K_{O2}[HPP]) + ([HPP][O_2])} \quad (1)$$

Determination of Ligand-Binding Constants. The binding constants for α-keto acid ligands were measured under anaerobic conditions according to the methods of Johnson-Winters et al. (*4*).

Oxygen Reactivity. The holoenzyme oxidation was measured as previously described (*4*). The holoenzyme complex (20 μM final) was mixed against varying pseudo-first-order concentrations of oxygen (195−948 μM) on a HI-TECH DX2 stopped-flow instrument. The rate constants measured from the fit of the increase in absorbance at 320 nm to a single exponential (k_{obs}) were plotted against oxygen concentration ($[O_2]$). The curve obtained was fit to eq 2 to determine the magnitude of the second-order rate constant for holoenzyme oxidation.

$$k_{obs} = k[O_2] \quad (2)$$

Pre-Steady-State Analysis Using Stopped-Flow Spectrometry. For reactions that used pseudo-first-order enzyme reactant stoichiometries, a tonometer was prepared with 2.01 mM AtHPPD, 2 mM Fe(II), and 4 mM HPP in 20 mM HEPES at pH 7.0 (1 mM AtHPPD·Fe(II)·HPP complex after mixing) and made anaerobic by 45 cycles of vacuum and argon at 4 °C. A cycle consisted of exposure to vacuum for 5−6 s to remove the exchanging gases and refilling the tonometer with argon at a regulated maximum pressure of 5 psi. After each set of three cycles, the enzyme and argon were allowed to equilibrate with gentle agitation for approximately two minutes. This was mixed with a 200 μM (100 μM final) oxygen solution at 5 °C and monitored with a stopped-flow fitted with a diode array collection device. Data were collected from 0.001 to 10 s. These data was rendered and analyzed using Specfit/32 Global Analysis System (Spectrum Software Associates, Chapel Hill, NC) and fit to the model depicted in Scheme 2.

Scheme 2

$$\text{HPPD} \cdot \text{Fe(II)} \cdot \text{HPP} + O_2 \xrightarrow{k_1} \text{I} \xrightarrow{k_2} \text{II} \xrightarrow{k_3} \text{HPPD} \cdot \text{Fe(II)} \cdot \text{HPP} + \text{HG} + CO_2$$

The reactions that used PPA were pseudo-first-order in oxygen and were prepared in an essentially equivalent manner as described above with a different reactant ratio. AtHPPD·Fe(II)·PPA complex was made to 200 μM concentration. This complex was mixed with 1900 μM oxygen, and spectral data were collected from 0.001 to 150 s. Data for individual wavelengths were analyzed using KinetAsyst software (HI-TECH scientific) and Spectfit/32.

Product Analysis for the Reaction of PPA with HPPD. AtHPPD was reacted with phenylpyruvic acid, and oxygen consumption was monitored with a Hansatech/Clarke-type oxygen electrode. The reactions contained varied amounts of AtHPPD with stoichiometric Fe(II) and saturated (on the

basis of K_d) PPA in 20 mM HEPES at pH 7.0. These reactions were quenched in 3.5% (v/v) TCA after the rate of consumption of dioxygen returned to background. The precipitated protein was removed with centrifugation at 23 000 *g* for 5 min. The supernatant (20 μL) was injected onto a reverse-phase Phenomenex phenyl column isocratically operating at 1 mL/min in an 80:20 mixture of 20 mM citrate at pH 3.5 and acetonitrile. Prior to analysis, standard curves for phenylacetate (PA) and 2HPA were made using the authentic compounds and the same HPLC conditions, monitoring at 260 nm with a Waters 2487 absorbance detector.

EPR of the PPA Inactivated Enzyme. Samples for EPR were prepared by forming 200 μM of the AtHPPD·Fe(II)·PPA complex in a tonometer using the methods described above. This sample was then opened to atmospheric oxygen at 4 °C. The samples at 30 and 2000 s were then withdrawn, placed in an EPR tube, and immersed in liquid nitrogen. EPR spectra were recorded using a Bruker EleXsys E500 EPR spectrometer equipped with an Oxford Instruments ITC4 temperature controller and an ESR-900 helium flow crystat. A Bruker ER-4116DM cavity was used with a resonant frequency of 9.63 GHz (in perpendicular mode), and field modulation at 100 kHz was employed. All other operating parameters for individual spectra are specified in the figure legends. The integration of the ferric iron signal was compared to a 2 mM Cu(II)SO_4 spin standard prepared in 20 mM EDTA at pH 7.0.

MS Analysis. AtHPPD (540 μM) and PPA-inactivated (~200 μM) AtHPPD were purified by HPLC using a Phenomenex C5 analytical column (4.6 × 150 mm). The PPA-inactivated enzyme was prepared by mixing the AtHPPD·Fe(II)·PPA complex (200 μM AtHPPD, 200 μM Fe(II), 4 mM PPA) with molecular oxygen (400 μM) at 5 °C and allowing it to react for 30 min. Elution of the proteins was achieved via a 40 min stepped gradient from Buffer A (H_2O, 0.1% trifluoroacetic acid) to Buffer B (CH3CN, 0.1% trifluoroacetic acid). The gradient used increased the fraction of Buffer B to 10% over the first 5 min followed by a hold for 5 min. The fraction of Buffer B was then increased to 30% over the next 5 min and held at this level for 10 min, followed by an increase to 70% of total mobile phase over the next 5 min and held at this level for another 10 min. Both the active and PPA inactivated proteins eluted at ~33.5 min. Both samples were then lyophilized. These fractions were redissolved in 100 μL of 49% methanol and 1% formic acid and analyzed by ESI-FTMS. For mass spectrometric analysis, a custom 8.5 T ESI-FTMS mass spectrometer was used, which was equipped with a front-end quadrupole (*40*). The samples were introduced into the FTMS instrument using a NanoMate 100 apparatus for automated nanospray (Advion Biosciences, Ithaca, NY). Typically, 500 ms ion accumulation per scan was used, and 50−200 scans were acquired per spectrum. The instrument was externally calibrated using ubiquitin with monoisotopic *Mr* value of 8560.65 Da (Sigma). For the calculation of the masses of the proteins, the MIDAS analysis datastation was used (*41*).

Inhibitor Binding Kinetics. The binding of 2-[2-nitro-4-(trifluoromethyl)benzoyl]-1,3-cyclohexanedione (NTBC) and 2-[4-(methylsulfonyl)-2-nitrobenzoyl]-1,3-cyclohexanedione (Mesotrione) was monitored under anaerobic conditions by stopped-flow spectrophotometry, observing the accumulation of charge-transfer absorbance (*34*). The anaerobic AtHPPD·Fe(II) complex (62.5 μM final concn) was mixed with varying pseudo-first-order concentrations of inhibitor (0.590−6.75 mM) that were made anaerobic by sparging with argon for 15 min. Once the two reactants were mixed, UV/visible spectra (300−700 nm) were collected with logarithmic time increments. The datasets were fit to the model depicted in Scheme 3 to obtain rate constants. Initial enzyme- and inhibitor-absorbance contributions were subtracted from the deconvoluted spectra of the charge-transfer species to obtain pure charge-transfer spectra.

Scheme 3

$$\text{HPPD} \cdot \text{Fe(II)} + \text{Inhibitor} \xrightarrow{k_{obs}} \text{HPPD} \cdot \text{Fe(II)} \cdot \text{Inhibitor}_{CT1} \xrightarrow{k_3} \text{HPPD} \cdot \text{Fe(II)} \cdot \text{Inhibitor}_{CT2}$$

For evidence of the degree of reversibility of inhibitor association, the oxidation of the HPPD·Fe(II)·NTBC or Mesotrione complex was monitored, observing the metal-to-ligand charge transfer on a long time scale when exposed to atmospheric dioxygen. A solution of 60 μM HPPD was made anaerobic in a 4 cm path length anaerobic cuvette by 45 exchanges of vacuum and argon. After the sample was made anaerobic, ferrous ammonium sulfate and inhibitor were each added to a final concentration of 55 μM from separate sidearms to form the 55 μM HPPD·Fe(II)·inhibitor complex. The solution was then exposed to atmospheric oxygen, and spectra were taken on a Cary 3 UV/Vis spectrophotometer over an 8 h period at 4 °C.

RESULTS

Expression and Purification. Two hours of induction of *E. coli* BL21 DE3 cells hosting the plasmid pET-HPP with 0.5 mM IPTG resulted in the formation of large quantities of inclusion-body protein and yielded only relatively small amounts of activity. However, uninduced control samples accumulated active AtHPPD for longer periods and produced less inclusion-body proteins (Figure 1). This suggested that the rate at which the induced cells synthesized protein was more rapid than the rate at which AtHPPD folded into the soluble, active-tertiary conformation. Leaky basal expression

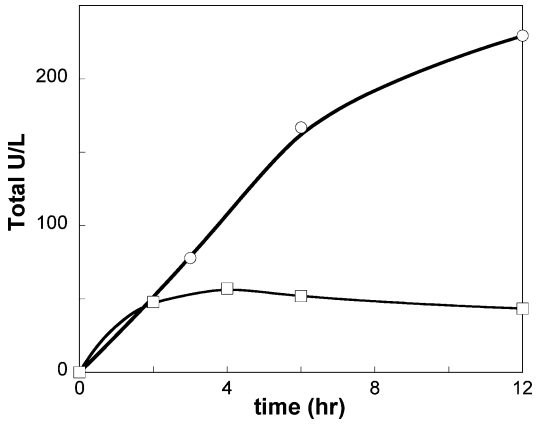

FIGURE 1: Expression of AtHPPD activity from *E. coli* BL21 DE3. Total activity/L vs time for IPTG induced (□) and uninduced (○) cells. At specific times after inoculation, the cells were harvested, sonicated, and centrifuged at 33 000*g* for 30 min. The supernatant was then assayed for AtHPPD activity. Activity was measured at 25 °C using an oxygen electrode. The conditions were 20 mM HEPES buffer at pH 7.0 in the presence of 25 μM Fe(II), 500 μM βME, and 400 μM HPP in atmospheric oxygen (~250 μM).

Table 1: Purification of AtHPPD

purification procedure	total protein (mg)	total activity (U/L)[a]	specific activity (U/mg)[a]
sonicate supernatant	380	189	0.50
Strep. supernatant (1.75%)	279	206	0.74
$(NH_4)_2SO_4$ supernatant (40%)	174	175	0.99
$(NH_4)_2SO_4$ pellet (50%)	61	97	1.58
IEC eluate	15	60	4.05
SEC eluate	13	47	3.53

[a] Measured at 25 °C and pH 7.0.

Table 2: Steady-State Kinetic Parameters for AtHPPD

parameter[a]	value
V_{max} (s^{-1})	0.065 ± 0.005
K_{HPP} (μM)	6.9 ± 1.9
K_{O2} (μM)	115 ± 26
V/K_{HPP} ($mM^{-1}\,s^{-1}$)	9.4 ± 1.0
V/K_{O2} ($mM^{-1}\,s^{-1}$)	0.56 ± 0.27

[a] Measured at 4 °C, with 0.5 μM AtHPPD, 0.5 μM ferrous ammonium sulfate, 0.5 mM βME, and 20 mM HEPES buffer at pH 7.0.

from the pET expression system in the absence of an externally applied inducing agent allows for a lower concentration of nascent folding protein at any point in time (*42*). It was empirically found that cells allowed to grow uninduced for 12 h maximized the activity to cell density ratio (data not shown). Using this method, a 5-fold increase to ~10 mg of active protein per liter of culture was obtained.

To efficiently purify the highly active enzyme, we adapted the published purification methods for *Streptomyces avermitilis* HPPD (*4*) and for *Arabidopsis* HPPD (*38*). The latter crystallographic study of AtHPPD did not quote activity; therefore, a direct comparison of the methods in terms of enzyme viability was not possible. A recent study of AtHPPD reports to have heterologously expressed a highly active enzyme in *E. coli*. The enzyme from this recent study had a specific activity approximately 100-fold lower than the one reported here (*43*). Table 1 summarizes the purification of AtHPPD. Overall, the method is 25% efficient. Unlike other HPPDs, the purified enzyme has no color (*8*, *10*, *44*). The enzyme is stable for several hours at room temperature, indefinitely at 4 °C, and can be concentrated to 100 mg/mL (3.4 mM).

Steady-State Kinetic Parameters. Both dioxygen and HPP were varied to determine the steady-state constants for AtHPPD at 4 °C (Table 2). At this temperature, AtHPPD has a turnover number of $0.065 \pm 0.005\ s^{-1}$. The K_m value of HPP with AtHPPD is $6.9 \pm 1.9\ \mu$M. The second substrate, oxygen, has a K_m value of $115 \pm 26\ \mu$M, indicating that the enzyme is ~80% saturated in oxygen under atmospheric conditions at 4 °C.

Binding Constants. The binding constants of HPP and PPA were determined by mixing the anaerobic holoenzyme complex with the anaerobic substrate and recording an absorbance spectrum for each concentration. For both HPP and PPA, the rate of binding and dissociation was sufficiently fast to reach equilibrium within the dead time of the stopped-flow instrument (~1.4 ms). The bidentate association of the α-keto acid portion of each ligand (HPP and PPA) with the active-site metal ion of the holoenzyme produces a charge-transfer feature around 500 nm. The λ_{max} value for this feature with HPP is 480 nm, which is slightly blue-shifted from the λ_{max} value of the charge transfer observed with SaHPPD, whose maximum was 490 nm (*4*). The charge-transfer feature of PPA with the holoenzyme has a λ_{max} value at 510 nm. This feature is red-shifted from the native substrate and is considerably different from the charge transfer associated with the complex of SaHPPD and PPA ($\lambda_{max} = 485$ nm). The K_d value of HPP with AtHPPD·Fe(II) is $29 \pm 7\ \mu$M, whereas the binding constant for PPA was determined to be $319 \pm 68\ \mu$M, both of which are similar to the binding constants for these ligands with SaHPPD (Figure 2) (*4*). For each ligand, the enzyme concentration was decreased by 15% in the analysis from that predicted by the extinction coefficient in order that the isotherm be positive at low ligand concentrations. This suggests that this fraction of the total enzyme active sites are unavailable to bind the substrate.

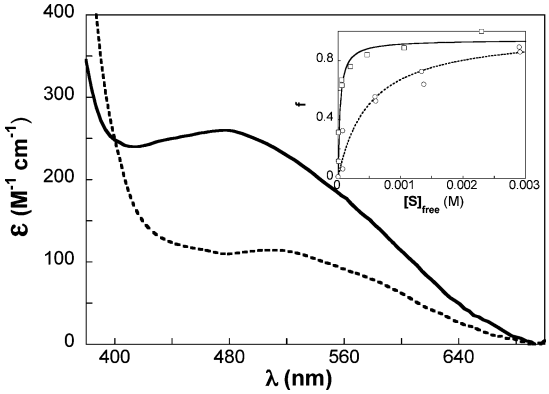

FIGURE 2: Charge-transfer absorbance spectra of HPP (—) and PPA (---) in complex with the holoenzyme under anaerobic conditions. Inset: binding isotherm for the titration of HPP (□) and PPA (○) vs 200 μM AtHPPD·Fe(II). The *f* represents fractional saturation of the enzyme. Data were fit to the single-site binding equation assuming 85% of sites available, measured at 4 °C in 20 mM HEPES at pH 7.0.

PPA Turnover Product Analysis. Oxygen consumption is observed upon the addition of PPA to a reaction mixture containing AtHPPD, Fe(II), the reductant βME, and HEPES buffer at pH 7.0. After acid quenching and centrifugation to remove the protein, the reaction mixture was injected onto an analytical phenyl column, and the components of the mixture were separated by HPLC. Phenylacetic acid (PA) and 2HPA production was monitored and compared to standard curves for these molecules measured under the same conditions using authentic compounds. For every three molecules of molecular oxygen consumed by the AtHPPD·Fe(II)·PPA complex, two molecules of phenylacetate were produced, and no other additional products were detected. In these reactions, oxygen consumption was observed to be stoichiometric with the enzyme concentration (Figure 3), and the enzyme was found to be completely inactive with the cessation of dioxygen consumption and did not resume turnover with further addition of PPA Fe(II) or reductant (data not shown). When the inactivated enzyme was dialyzed for 2 h (2.0 vs 2000 mL at 4 °C) and re-assayed, 4% of the initial activity with HPP as a substrate was observed. These data suggest that HPPD does not use PPA as a substrate in normal plant metabolism.

Holoenzyme Oxygen Reactivity. The order of the addition of substrates to the enzyme in catalysis can be confirmed

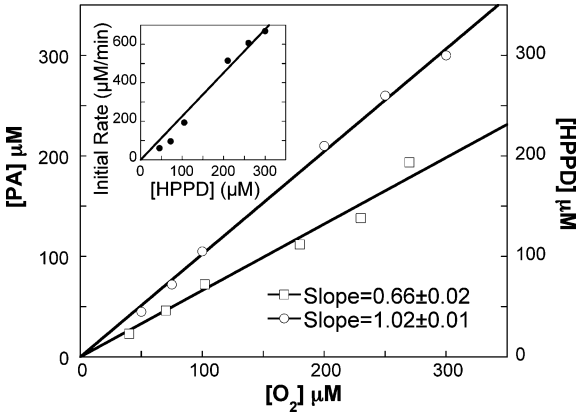

FIGURE 3: Uncoupling and processivity of AtHPPD in the presence of PPA. AtHPPD was reacted with PPA and oxygen consumption was monitored using an oxygen electrode at 25 °C in 20 mM HEPES buffer at pH 7.0 with Fe(II) concentrations equal to that of the enzyme: 500 μM βME and 4 mM PPA. The AtHPPD concentration vs molecular oxygen consumption (○) when reacted with PPA and the phenylacetate (PA) production vs total oxygen consumption (□) was identified using HPLC. Detection was at 260 nm on a Phenomenex phenyl column (4.6 × 250 mm) isocratically operating at 1 mL/min in an 80:20 mixture of 20 mM citrate at pH 3.5 and acetonitrile. The inset shows the dependence of the initial rate of dioxygen consumption on the concentration of AtHPPD.

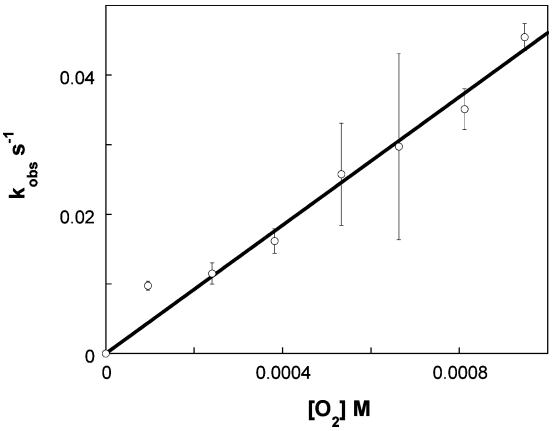

FIGURE 4: Oxidation of AtHPPD·Fe(II) complex in the presence of dioxygen monitored at 320 nm. Varied oxygen concentrations were mixed with anaerobic holoenzyme (12.5 μM AtHPPD, 10 μM Fe(II) final concn) at 4 °C.

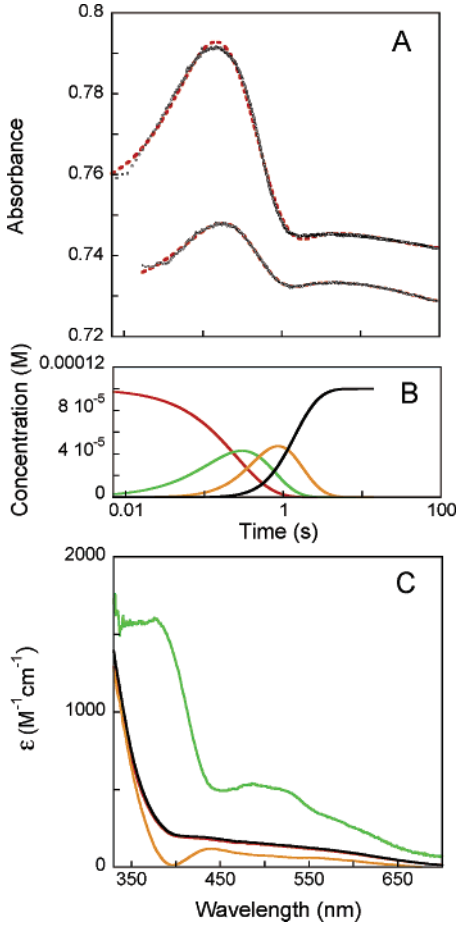

FIGURE 5: Stopped-flow kinetic analysis of AtHPPD using pseudo-first-order reactant stoichiometry in the presence of saturated HPP. This figure shows data traces when AtHPPD·Fe(II)·HPP (1.05 mM AtHPPD, 1.0 mM Fe(II), and 2.0 mM HPP) was mixed with dioxygen (100 μM) in 20 mM HEPES buffer at pH 7.0 at 5 °C. (A) Stopped-flow data traces at 380 nm (upper) and 490 nm (lower) with overlaying fits of the model in Scheme 3; k_1 = 9 000 M^{-1} s^{-1}, k_2 = 2.76 s^{-1}, and k_3 = 0.065 s^{-1} (B) Fractional accumulation of intermediate species on the basis of reactant concentrations and rate constants: oxygen, red; intermediate I, green; intermediate II, orange; and product formation, black. (C) Intermediate spectra (300−700 nm) deconvoluted from photodiode array data sets of the reaction above. The colors match those used in the reactant concentration profile above.

by observing the reactivity of the holoenzyme with molecular oxygen in the absence of the native substrate, HPP. When the holoenzyme reacts with molecular oxygen, there is an increase in the absorbance spectrum at 320 nm from the oxidation of Fe(II) to Fe(III) ($\Delta\epsilon_{320nm}$ = 1400 M^{-1} cm^{-1}). The rate constant for the formation of this feature was measured in the presence of a range of pseudo-first-order dioxygen concentrations ranging from 0.095 to 0.948 mM. The data obtained indicated a good fit for a line that intersects the origin whose slope gave a second-order rate constant of 46.1 ± 1.5 M^{-1} s^{-1} (Figure 4). This value would only support the turnover number when the dioxygen concentration was in excess of 2 mM. This indicates that oxygen reacts slowly without complexation with the holoenzyme (vide infra). This is in agreement with the hypothesis that the substrate HPP acts to heighten the reactivity of the iron atom toward molecular oxygen when bound to the holoenzyme complex (*4*).

Pre-Steady-State Analysis. Figure 5 summarizes the reaction of the AtHPPD·Fe(II)·HPP complex (1 mM final) with dioxygen (100 μM final concn) as observed by rapid-mixing absorbance measurements. The viscosity of the concentrated enzyme solution gave Schlieren mixing artifacts that limited data analysis to that which was collected beyond 10 ms. As such, absorbance data were analyzed from 0.01 to 100 s. For the majority of wavelengths, data traces show an initial absorbance increase with a rate constant (k_1) of 9090 ± 230 M^{-1} s^{-1} followed by a decrease with a rate constant (k_2) of 2.7 ± 0.2 s^{-1}. The third rate constant (k_3) is observed as a small increase at most wavelengths with a rate constant of 1.2 ± 0.1 s^{-1} (Figure 5). The final phase (k_4) is slow, relative to turnover and was not assigned to a normal catalytic event. It is observed as a small amplitude decrease at most wavelengths with a rate constant of 0.0197 ± 0.002 s^{-1}. The spectrum of intermediate I closely resembles the spectrum of the first intermediate observed for the reaction of HPPD from SaHPPD in the presence of HPP and dioxygen. Intermediate II is less strongly absorbing than the spectrum at time zero and decays to yield a spectrum equivalent to

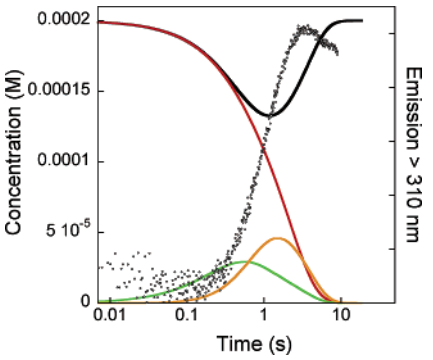

FIGURE 6: Fluorescence accumulation >310 nm when excited at 305 nm during a single turnover of AtHPPD·Fe(II)·HPP (205 μM AtHPPD, 200 μM Fe(II), and 2 mM HPP) with dioxygen (200 μM). The fractional accumulation of intermediate species on the basis of reactant stoichiometries and rate constants is overlayed with the fluorescence data: oxygen, red; intermediate I, green; intermediate II, orange; and AtHPPD·Fe(II)·HPP, black.

the time zero spectrum (Figure 5C) suggesting that the decay of the second intermediate occurs concomitantly with re-association of the substrate to re-form the characteristic ferrous holoenzyme to HPP charge-transfer band.

Further evidence for the nature of intermediate II was obtained from observation of fluorescence changes during the course of a single turnover. The HG product is approximately 11-fold more fluorescent than the HPP substrate when excited at wavelengths between 270 and 310 nm (*7*). As such, it is possible to independently identify which process observed in absorbance experiments is involved in the formation of the product. To limit changes in the incident- and emitted-light inner filter, the reaction was excited at 305 nm, where the extinction coefficient of HPP and HG are similar. The anaerobic holoenzyme−substrate complex (205 μM AtHPPD, 200 μM Fe(II), and 2 mM HPP) was mixed with 200 μM dioxygen, and the emission beyond 320 nm was observed (Figure 6). The data show that the primary increase in fluorescence occurs with the accumulation of intermediate II, strongly suggesting that this intermediate is HG in complex with the ferrous enzyme, equivalent to intermediate III observed in single turnover reactions of SaHPPD with HPP (*7*). The rate constant determined from the fit of the data to the model depicted in Scheme 2, where both k_1 and k_3 were fixed to the values measured in absorbance based pseudo-first-order experiments, gave a value of 3.50 ± 0.15 s^{-1}, consistent with this phase corresponding to k_2.

We also examined the reaction of AtHPPD·Fe(II)·PPA complex with dioxygen using rapid-mixing methods. The reaction in which the dioxgen was the limiting pseudo-first-order reactant (1mM AtHPPD·Fe(II)·PPA, final mixed against 100 μM dioxygen final) was hampered by photoreactivity of the excess AtHPPD·Fe(II)·PPA complex. After an initial increase, all data traces included a slow decrease that continued beyond 3000 s. It was concluded that this was artifactual because the decrease continued to bleach the sample well outside of the time frame of inactivation and below the absorbance of 90% of the enzyme, which does not react with dioxygen under this reactant stoichiometry. However, the reaction of AtHPPD in the presence PPA with dioxygen is stoichometric with dioxygen, renders the enzyme inactive, and does not involve multiple turnovers (Figure 3). Therefore, the reaction of limiting AtHPPD·Fe(II)·PPA complex (100 μM) with a pseudo-first-order oxygen concentration (1 mM final) consumes only stoichiometric quantities of dioxygen. Figure 7 depicts the reaction of 1 mM dioxygen with 100 μM AtHPPD·Fe(II)·PPA. This reaction was spectrally monitored at all wavelengths from 300 to 700 nm for 285 s using a diode-array collection device coupled to the stopped-flow spectrophotometer. A monophasic increase in absorbance was observed at wavelengths from 300 to 500 nm. From the fit of the data to an exponential, the rate constant associated with this event was determined to be 0.035 ± 0.002 s^{-1}. The reaction appears complete within 200 s, and no further absorbance changes in the 300−500 nm region are observed to 1000 s. The deconvoluted absorbance spectra of the species involved indicate the formation of an absorbance band centered around 355 nm (Figure 7B). The difference spectrum obtained by subtracting the initial (time zero) absorbance spectrum from the final spectrum shows the formation of a transition with an extinction coefficient of ~1 300 M^{-1} cm^{-1}(Figure 7C). An examination of longer wavelengths indicate the formation of weak transitions with an absorbance maximum at 670 nm (Figure 7C). These transitions give the reaction an emerald green color.

EPR Spectra of PPA Inactivation. EPR spectra representing 30 and 2000 s after the exposure of 200 μM AtHPPD·Fe(II)·PPA complex to dioxygen (~400 μM) suggest that the inactivation of AtHPPD in the presence of this ligand results from the oxidation of the active-site metal ion (Figure 7D). As the reaction progresses, the intensity of the $g = 4.3$ feature increases. The quantitative integration of Fe(III) signals is notoriously difficult (*45* and references therein); however, a comparison of the PPA inactivated spectra to a 2 mM Cu(II)-EDTA standard at pH 7.0 did produce Fe(III) concentrations largely consistent with the complete oxidation of the sample. For the 30 s sample at 5 K, integration suggests total Fe(III) > 0.12 mM, and for the 2000 s spectrum, total Fe(III) is >0.13 mM. However, an examination of these spectra appear to indicate that the 2000 s spectrum is significantly more intense than the 30 s spectrum and thus that the direct comparative integration was fundamentally flawed in some way (Figure 7). An alternative approach was tried, where the contributions to the spectra from the $g \sim 4.3$ lines were measured, and these integrated to 40 μM for the 30 s sample and 63 μM for the 2000 s sample. Applying a somewhat arbitrary contribution of MS $= |\pm 3/2\rangle = 1/3$, these suggest [Fe(III)] ≥ 0.12 mM for the 30 s sample and [Fe(III)] ≥ 0.19 mM for the 2000 s sample. At 15 K, the 2000 s sample returned the total Fe(III) concentration by direct integration of >0.17 mM, and the integration of the $g \sim 4.3$ line indicated 72 mM spins, suggesting total [Fe(III)] ≥ 0.22 mM. Taken together, reasonable estimates for [Fe(III)] would be ≥ 0.1 mM for the 30 s sample and ≥ 0.2 mM for the 30 min sample. These data are generally consistent with the fraction of conversion expected from kinetic observations of inactivation in the presence of PPA and strongly suggest that the oxidation of the metal ion is one contribution to a process that renders the enzyme inactive.

An additional relatively low intensity (~10%) free radical is observed at $g = 2.0$. This signal does not significantly change during inactivation and is consistent with a tyrosyl radical (*46*−*48*). The active site of AtHPPD, however, has

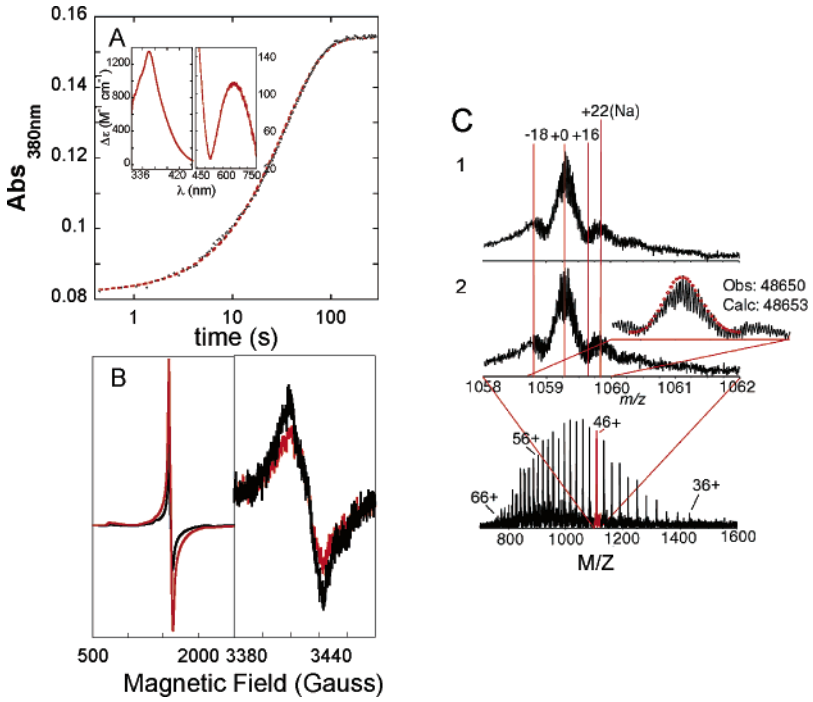

FIGURE 7: Inactivation by dioxygen in the presence of phenylpyruvate. (A) Monophasic data trace and fit (----) of anaerobic AtHPPD·Fe(II)·PPA complex (95 μM final concn) mixed vs pseudo-first-order oxygen (950 μM final concn) monitoring at 380 nm. Inset: difference spectra (final − intial). Left plot: difference spectrum (320−440 nm) and right plot: expansion of difference spectra (440−800 nm). (B) EPR spectra of AtHPPD 30 s (black) and 2000 s (red) after reacting with molecular oxygen in the presence of PPA. The anaerobic reaction mixture of AtHPPD (205 μM), Fe(II) (200 μM), and PPA (4 mM) was open to atmospheric oxygen at 4 °C (385 μM) and pH 7.0. Left plot: spectra taken at 10 K, where $\nu = 9.631$ GHz, $p = 5.016$ mW, $A_m = 14$ G, and $NS = 9$; right plot: the same sample was warmed to 40 K, and the power was reduced ($p = 1.001$ mW). Other experimental parameters $\nu = 9.631$, $A_m = 1$ G, and $NS = 40$. (C) Mass spectra of (1) active AtHPPD and (2) PPA inactivated AtHPPD. Inset: observed mass data (black) and fit (red) to the predicted molecular mass of AtHPPD that has a posttranslationally cleaved *N*-terminal methionine.

no tyrosine residues within 10 Å of the active-site metal ion (*38*). This small fraction does not correlate with the 66% yield of the PA product and suggests self hydroxylation of the enzyme at some stage during expression or purification, prior to PPA inactivation. This tyrosine fraction of the PPA-inactivated enzyme can then reduce the ferric ion to form the phenolic radical during inactivation (*49*).

Mass Spectral Analysis of the Inactivated Enzyme. Both PPA-inactivated HPPD and the enzyme as isolated were subject to mass spectral analysis to determine molecular weight (Figure 7C, 46+ charge state shown). The masses of the proteins were found to be within 3 ± 1 mass units of the mass expected (48650 Da) for posttranslational *N*-terminal methionine removal from AtHPPD. Both samples show some evidence of a +16 mass unit fraction that can be best modeled to ~5% of sample, and this fraction may account for the small fraction of the apparent tyrosyl radical observed in the EPR data (vide supra). Reconciling the total loss of activity and an apparent inability to reactivate the enzyme with ±1 change in mass leads to two possible explanations. The first is that covalent modification of the enzyme occurs prior to the bifurcation reaction that yields two-thirds of the decarboxylated, phenylactate product and that this modification does not survive mass spectral analysis. The second possibility is that the covalent modification results in an increase in mass of 1 Da (under the acidic conditions used), such as in the conversion of an amide side chain to an acid (Gln→Glu, Asn→Asp) with the displacement of ammonia. This latter possibility was ruled out by the observation that no NADPH consumption is observed when αKG and excess glutamate dehydrogenase activity are added to the HPPD/PPA inactivation reaction (data not shown).

Inhibitor Binding and Dissociation Kinetics. It has been crystallographically and spectrally shown that the triketone inhibitor associates in a bidentate arrangement with the Fe(II) atom bound to the HPPD active site (*34*, *35*, *38*, *50*). Stopped-flow spectrophotometry was utilized to observe the rates of association of both NTBC and Mesotrione with AtHPPD. The anaerobic holoenzyme complex (62.5 μM final concn) was mixed against various pseudo-first-order concentrations of the anaerobic inhibitor (0.5−6.73 mM final concn). The increase in absorbance due to metal-to-ligand charge transfer upon the mixing of the holoenzyme and the inhibitor was monitored from 0.001 to 100 s. The kinetic data obtained for NTBC and Mesotrione are remarkably similar. At all concentrations, a biphasic increase was observed (Figure 8A). The rate constant associated with the first of these phases hyperbolically titrated with the inhibitor concentration to an asymptote of 12−16 s^{-1}, indicating weak binding constants of 937 ± 101 μM for NTBC and 602 ± 108 μM for Mesotrione, prior to the appearance of the first charge-transfer absorbance. The rate constant associated with the second phase was independent of inhibitor concentration (~0.6 s^{-1}). These data indicate that the mechanism of binding of triketone inhibitors to AtHPPD is entirely consistent with the previous inhibitor binding mechanism proposed by Kavana and Moran for NTBC binding to SaHPPD (*34*). Moreover, the association of both inhibitors is ostensibly irreversible and suppresses dioxygen reactivity of the metal ion because no evidence of loss of the ferrous ion to inhibitor

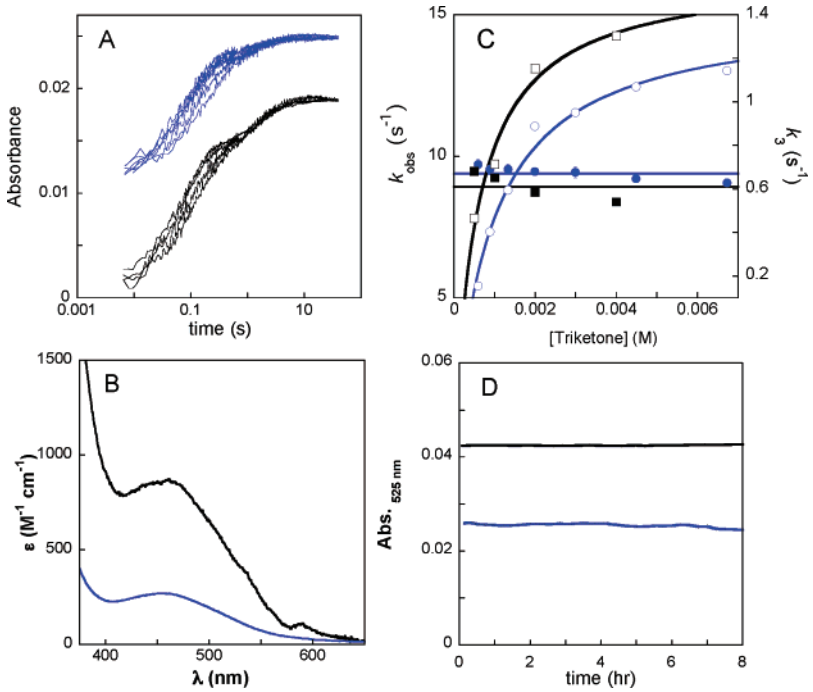

FIGURE 8: Inhibitor-binding kinetics monitoring the formation of the metal-to-ligand charge-transfer bands of the inhibitor−AtHPPD complex for NTBC (blue) and Mesotrione (black). (A) Kinetics of binding of NTBC and Mesotrione to AtHPPD·Fe(II) (62.5 μM final concn). The holoenzyme complex was mixed with varied inhibitor concentrations (0.590− 6.73 mM NTBC; 0.5−4.0 mM Mesotrione) and monitored at 475 nm at 4 °C in 20 mM HEPES at pH 7.0. (B) Difference spectra of NTBC and Mesotrione bound to AtHPPD·Fe(II) (200 μM) in 20 mM HEPES at pH 7.0. (Inhibitor and holoenzyme contributions were subtracted.) (C) Observed rate constants, k_{obs} (○, □) and k_3 (●, ■) for NTBC (○) and Mesotrione (□) are plotted vs inhibitor concentration from a two exponential fit of the original data traces in A. (D) Monitoring the stability of the charge-transfer absorbance at 525 nm of the AtHPPD·Fe(II)·NTBC and Mesotrione complexes. The complex was made anaerobic and then opened to atmospheric oxygen for an 8 h period.

charge transfer is observed under conditions of atmospheric oxygen at 4 °C.

DISCUSSION

HPPD catalyzes the first committed step of tyrosine catabolism. The function of this reaction is to further activate the aromatic ring of HPP to make it more susceptible to cleavage. Early research of the enzyme was concerned with the mechanism to gain an understanding of the rather intriguing conversion that produces HG from HPP (Scheme 1), a reaction that involves decarboxylation, aromatic oxygenation, and substituent migration (*13*, *15*, *18*, *51*−*53*). For the last two decades, however, the inhibition of HPPD has been the area of primary research interest. This has been a consequence of the key role of HPPD in a number of rare diseases in mammals and in the production of redox cofactors vital to photosynthesis in plants (*27*, *31*, 54−57). HPPD inhibitors have proven very effective as drugs and herbicides because of their tight, specific association with their target, low toxicity in animals, and high stability. It could be argued that the two inhibitors of greatest prominence are NTBC, which is sold as Nitisinone by Orphan Pharmaceuticals for the treatment of tyrosine catabolism defects (*25*) and Mesotrione, which is a broad-leaf-selective herbicide sold as Callisto by Syngenta (*23*).

Despite the fact that a number of X-ray crystal structures of plant HPPDs have been published, in the presence and absence of inhibitory molecules (*38*, *58*), no study has yet conducted a comprehensive kinetic characterization of plant HPPD with regard to catalysis or inhibition. The data obtained in this study indicate that with the exception of the reaction of the enzyme with PPA, AtHPPD behaves in a manner very similar to the form from *Streptomyces* (*4*, *7*, *34*).

The reaction mechanism of HPPD has had relatively little published to support the identity of catalytic intermediates. Recently, three intermediates were observed in a single turnover with the enzyme from *Streptomyces* (*7*). Evidence from stopped-flow fluorescence and kinetic isotope effects suggest that the third intermediate was the complex of the enzyme with the product HG and that the release of HG is rate-determining in turnover. On the basis of kinetic isotope effects with ring deuterated HPP, the identity of the second intermediate is likely to be either an epoxide-like species or a nonaromatic dienone of the product. In this earlier study, no evidence was found for the identity of the first intermediate. Two intermediates can be observed to accumulate in a single turnover reaction of AtHPPD, and these would appear to be equivalent to intermediates I and III, observed with SaHPPD. The spectrum of the first and most strongly absorbing intermediate is the same as that observed with SaHPPD (*7*). However, the rate constant for the formation of this intermediate is an order of magnitude slower, and maximum accumulation occurs around 200 ms under the reaction conditions used (Figure 5). The increase in fluorescence associated with the accumulation of the second intermediate is suggestive of HG complex formation in this phase (Figure 6). The decay of this complex is also the rate-limiting process of turnover with AtHPPD. In the presence of excess substrate, the release of product is observed as the re-formation of the spectrum of the charge transfer associated with the ferrous enzyme−HPP complex (Figure 5C).

Scheme 4

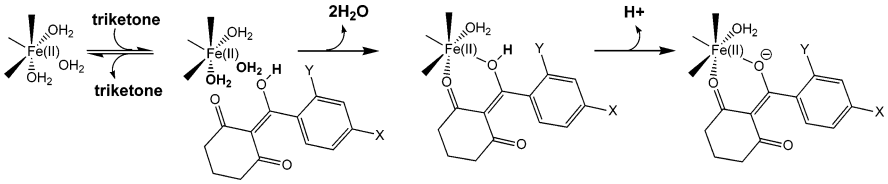

AtHPPD monophasically reacts with PPA in a noncatalytic event that results in the stoichiometric, with respect to dioxygen, irreversible inactivation of the enzyme. The reaction is bifurcated and decarboxylates two-thirds of the bound PPA to produce phenylacetate (Figures 3 and 7) and is first-order with respect the enzyme concentration (inset in Figure 3). The inactivated enzyme is in the Fe(III) oxidation state and has the same molecular weight within error as the active enzyme as isolated (Figure 7). This latter observation is most unexpected because the PPA-inactivated enzyme resists all attempts at reactivation, strongly suggesting that inactivation is a result of some covalent chemical transformation. As such, the fates of 66 % of the oxygen atoms that enter the reaction are unknown. However, the majority of bound PPA is decarboxylated, and presumably, this reaction is analogous to the decarboxylation of HPP in the production of the homogentisate. However, in the absence of more definitive evidence for the inactivation reaction, we are inclined not to draw speculative mechanistic conclusions. What is clear is that PPA is not a substrate for AtHPPD.

A number of research articles and texts have described a secondary role of HPPD in the conversion of PPA to 2-hydroxyphenylacetic acid (*8*−*18*). However, the majority of these studies (8/11) offered as evidence the results of assay methods that either monitored the depletion of PPA or detected the release of $^{14}CO_2$ from the PPA labeled at the carboxylate and did not directly establish the production of the 2-hydroxyphenylacetic acid. Furthermore, the HPPD used in these assays was either crude or of unknown concentration so that the processivity and/or catalytic function of the enzyme with respect to this ligand could not be established. Two studies have verified 2-hydroxphenylacetic acid production from preparations of mammalian HPPD (vide supra) (*13*, *15*).

An examination of the literature associated with 2HPA indicates that it is a dead-end product that has no metabolic role in any organism, and PPA, in all probability, is not a native substrate for HPPD (*59*). The evidence for this in bacteria is that *E. coli* cannot grow when 2-hydroxyphenylacetic acid is offered as the sole carbon source (*60*) and also that HPPD from *S. avermitlis* does not produce 2-hydroxyphenylacetic acid (*4*). Indirect evidence would suggest, however, that under abnormal conditions mammalian HPPD can convert PPA to 2-hydroxyphenylacetic acid. In mammalian metabolism, phenylketonuria (PKU) results from a deficiency of phenylalanine hydroxylase activity (*61*). The excess phenylalanine is converted to PPA by aminotransferase enzymes. Early studies in human subjects with PKU determined that the accumulation of phenylalanine in the blood directly correlated with increased excretion of 2-hydroxyphenylacetic acid in urine; this strongly implicated PPA as the metabolic intermediate (*62*). However, the proportion of total phenylalanine to be converted to 2-hydroxyphenylacetic acid was ∼10% of the dietary intake, which suggested that PPA is a less than optimal substrate for mammalian HPPD. This is consistent with the primary manifestation of PKU, the accumulation and excretion of PPA (*13*). Having examined two pure and highly active forms of HPPD in some detail, we suggest that PPA is generally not a substrate for HPPD from plants or bacteria and is, in all probability, not a native metabolic substrate for any form of HPPD.

Tyrosine catabolism has a unique and vital role in plant metabolism. A branch in the pathway from HG yields plastoquinone that is required both for photosystem function and also carotenoid pigment synthesis as the cofactor of phytoene desaturase (*19*). HPPD catalyzes the step of tyrosine catabolism that produces HG and, thus, is a particularly good target for herbicide development. There are at least three commercially available herbicides that target the inhibition of HPPD. The primary herbicide of this type for sale in the United States is Callisto and contains the active ingredient Mesotrione (Chart 1). Mesotrione is appropriate for herbicide use in maize because it specifically inhibits broad-leaf plants (*23*). In addition, it has a relatively short half-life in mammalian metabolism (*26*), high stability, and very low toxicity (*63*). The common moiety of these inhibitors is a 1,3-diketone that forms a bidentate association with the active-site Fe(II) metal ion of HPPD, physically preventing access of the substrate and suppressing dioxygen reactivity at the metal ion (*34*, 35). The recent observation that the triketone inhibitor NTBC associates with HPPD from *Streptomyces* in three steps, the last two of which are irreversible, and forms metal-to-ligand charge transfer (*34*) was at odds with much of the literature that had assumed simple reversible single-step binding to measure IC_{50} values with HPPD. Because HPPD from *Streptomyces* is not a normal or intended target of such inhibitors, verification of the observations made in this earlier investigation seemed warranted. Plant HPPD is the primary target of all such di and triketone inhibitors, including the drug NTBC, which was originally developed and patented for herbicidal purposes (*25*). Thus, AtHPPD is an appropriate form of this enzyme from which to establish whether the earlier observations made with NTBC and HPPD from *Streptomyces* apply more generally. To investigate the kinetic mechanism of binding for NTBC and Mesotrione inhibitiors, rapid-mixing experiments were conducted in which the anaerobic holoenzyme and anaerobic inhibitor were mixed. These data indicate an association mechanism equivalent to that proposed by Kavana and Moran (Scheme 4) (*34*), where a weak pre-equilibrium precedes the formation of two metal-centered binding events, both of which produce charge transfer.

NTBC was found to be irreversibly associated with HPPD from *Streptomyces*. This was the observation that ultimately lead to solving the crystal structure of the ferrous holoenzyme of SaHPPD with NTBC bound. The AtHPPD·Fe(II) complex was found also to be irreversibly associated with NTBC and

Mesotrione (Figure 8D). This observation is congruent with the proposal of Brownlee et al., where it was noted that with one exception all of the residues in the active site to contact the inhibitor were fully conserved and that species selectivity would therefore derive from bio-processing of the various triketones and not differences in HPPD structure across kingdoms (*35*).

ACKNOWLEDGMENT

We express our sincere thanks to Dr. Dean Della Penna and Maria E. Magallanes-Lundback from the Department of Biochemistry and Molecular Biology at Michigan State University for supplying the AtHPPD expression construct. We also express thanks to Dr. Brian Bennett of the National Biomedical EPR Center for collecting EPR spectra of the PPA-reacted AtHPPD enzyme. The center is funded by NIH P41 EB001980. Thanks is also due to Pieter Dorrestein of the Department of Chemistry, University of Illinois, Urbana−Champaign for mass spectral analysis of apo and PPA-inactivated forms of AtHPPD.

REFERENCES

1. Hausinger, R. P. (2004) FeII/alpha-ketoglutarate-dependent hydroxylases and related enzymes, *Crit. Rev. Biochem. Mol. Biol. 39*, 21−68.
2. Serre, L., Sailland, A., Sy, D., Boudec, P., Rolland, A., Pebay-Peyroula, E., and Cohen-Addad, C. (1999) Crystal structure of *Pseudomonas fluorescens* 4-hydroxyphenylpyruvate dioxygenase: an enzyme involved in the tyrosine degradation pathway, *Structure Fold Des. 7*, 977−988.
3. Neidig, M. L., Kavana, M., Moran, G. R., and Solomon, E. I. (2004) CD and MCD studies of the non-heme ferrous active site in (4-hydroxyphenyl)pyruvate dioxygenase: correlation between oxygen activation in the extradiol and alpha-KG dependent dioxygenases, *J. Am. Chem. Soc. 126*, 4486-4487.
4. Johnson-Winters, K., Purpero, V. M., Kavana, M., Nelson, T., and Moran, G. R. (2003) (4-Hydroxyphenyl)pyruvate dioxygenase from *Streptomyces avermitilis*: the basis for ordered substrate addition, *Biochemistry 42*, 2072−2080.
5. Moran, G. R. (2005) 4-Hydroxyphenylpyruvate dioxygenase, *Arch. Biochem. Biophys. 433*, 117−128.
6. Guroff, G., Daly, J. W., Jerina, D. M., Renson, J., Witkop, B., and Udenfriend, S. (1967) Hydroxylation-induced migration: the NIH shift, *Science 157*, 1524−1530.
7. Johnson-Winters, K., Purpero, V. M., Kavana, M., and Moran, G. R. (2005) Accumulation of multiple intermediates in the catalytic cycle of (4-hydroxyphenyl)pyruvate dioxygenase from streptomyces avermitilis, *Biochemistry 44*, 7189−7199.
8. Lindstedt, S., Odelhog, B., and Rundgren, M. (1977) Purification and some properties of 4-hydroxyphenylpyruvate dioxygenase from *Pseudomonas sp*. P. J. 874, *Biochemistry 16*, 3369−3377.
9. Lindstedt, S., and Rundgren, M. (1982) Blue color, metal content, and substrate binding in 4- hydroxyphenylpyruvate dioxygenase from *Pseudomonas sp*. strain P. J. 874, *J. Biol. Chem. 257*, 11922−11931.
10. Lindblad, B., Lindstedt, G., Lindstedt, S., and Rundgren, M. (1977) Purification and some properties of human 4-hydroxyphenylpyruvate dioxygenase (I), *J. Biol. Chem. 252*, 5073−5084.
11. Rundgren, M. (1977) Multiple forms of human 4-hydroxyphenylpyruvate dioxygenase (II), *J. Biol. Chem. 252*, 5085−5093.
12. Goodwin, B. L. (1972) *Tyrosine Catabolism*, Oxford University Press: New York.
13. Taniguchi, K., and Armstrong, M. D. (1963) The enzymatic formation of o-hydroxyphenylacetic acid, *J. Biol. Chem. 238*, 4091−4097.
14. Denum, J., Lindstedt, S., and Rundgren, M. (1982) in *Oxidases and Related Redox Systems* (King, T. E., Mason, H. S., and Morrison, M., Eds.) pp 519−542, Pergamon Press, Albany, NY.
15. Taniguchi, K., Kappe, T., and Armstrong, M. D. (1964) Further studies on phenylpyruvate oxidase occurrence of side chain rearrangement and comparison with p-hydroxyphenylpyruvate oxidase, *J. Biol. Chem. 239*, 3389−3395.
16. Lindstedt, S., and Rundgren, M. (1982) Inhibition of 4-hydroxyphenylpyruvate dioxygenase from *Pseudomonas sp*. strain P. J. 874 the enol tautomer of the substrate, *Biochim. Biophys. Acta 704*, 66−74.
17. Wada, G. H., Fellman, J. H., Fujita, T. S., and Roth, E. S. (1975) Purification and properties of avian liver p-hydroxyphenylpyruvate hydroxylase, *J. Biol. Chem. 250*, 6720−6726.
18. Rundgren, M. (1977) Steady-state kinetics of 4-hydroxyphenylpyruvate dioxygenase from human liver (III), *J. Biol. Chem. 252*, 5094−5099.
19. Goodwin, T. W., and Mercer, E. I. (1983) *Introduction to Plant Biochemistry*, 2nd ed., Pergamon Press, Sydney, Australia.
20. Hellyer, R. (1968) The occurrence of beta-triketones in the steam-volatile oils of some myrtaceous Australian plants, *Aust. J. Chem. 21*, 2825−2828.
21. Romagni, J. G., Meazza, G., Nanayakkara, N. P., and Dayan, F. E. (2000) The phytotoxic lichen metabolite, usnic acid, is a potent inhibitor of plant p-hydroxyphenylpyruvate dioxygenase, *FEBS Lett. 480*, 301−305.
22. Gray, R. A., Russay, R. J., and Tseng, C. K. US Patent (1980) pp 202, 840.
23. Mitchell, G., Bartlett, D. W., Fraser, T. E., Hawkes, T. R., Holt, D. C., Townson, J. K., and Wichert, R. A. (2001) Mesotrione: a new selective herbicide for use in maize, *Pest. Manag. Sci. 57*, 120−128.
24. Schulz, A., Ort, O., Beyer, P., and Kleinig, H. (1993) SC-0051, a 2-benzoyl-cyclohexane-1,3-dione bleaching herbicide, is a potent inhibitor of the enzyme p-hydroxyphenylpyruvate dioxygenase, *FEBS* Lett *318*, 162−166.
25. Michaely, W. J., and Kratz, G. W. (1988) U.S. Patent 780,127.
26. Hall, M. G., Wilks, M. F., Provan, W. M., Eksborg, S., and Lumholtz, B. (2001) Pharmacokinetics and pharmacodynamics of NTBC (2-(2-nitro-4-fluoromethylbenzoyl)-1,3-cyclohexanedione) and mesotrione, inhibitors of 4-hydroxyphenyl pyruvate dioxygenase (HPPD) following a single dose to healthy male volunteers, *Br. J. Clin. Pharmacol. 52*, 169−177.
27. Lindstedt, S., Holme, E., Lock, E. A., Hjalmarson, O., and Strandvik, B. (1992) Treatment of hereditary tyrosinaemia type I by inhibition of 4- hydroxyphenylpyruvate dioxygenase [see comments], *Lancet 340*, 813−817.
28. Garrod, E. A. (1902) The incidence of alkaptonuria: a study in clinical individuality, *Lancet* , 1616−1620.
29. Garrod, A. E. (1908) The croonian lectures on inborn errors of metabolism. Lecture II. Alkaptonuria, *Lancet* , 73−79.
30. Phornphutkul, C., Introne, W. J., Perry, M. B., Bernardini, I., Murphey, M. D., Fitzpatrick, D. L., Anderson, P. D., Huizing, M., Anikster, Y., Gerber, L. H., and Gahl, W. A. (2002) Natural history of alkaptonuria, *N. Engl. J. Med. 347*, 2111−2121.
31. Suwannarat, P., O'Brien, K., Perry, M. B., Sebring, N., Bernardini, I., Kaiser-Kupfer, M. I., Rubin, B. I., Tsilou, E., Gerber, L. H., and Gahl, W. A. (2005) Use of nitisinone in patients with alkaptonuria, *Metabolism 54*, 719−728.
32. Secor, J. (1994) Inhibition of barnyardgrass 4-hydroxyphenylpyruvate dioxygenase by sulcotrione, *Plant* Physiol. *106*, 1429−1433.
33. Pallett, K. E., Cramp, S. M., Little, J. P., Veerasekaran, P., Crudace, A. J., and Slater, A. E. (2001) Isoxaflutole: the background to its discovery and the basis of its herbicidal properties, *Pest. Manag. Sci. 57*, 133−142.
34. Kavana, M., and Moran, G. R. (2003) Interaction of (4-hydroxyphenyl)pyruvate dioxygenase with the specific inhibitor 2-[2-nitro-4-(trifluoromethyl)benzoyl]-1,3-cyclohexanedione, *Biochemistry 42*, 10238−10245.
35. Brownlee, J., Kayunta, J.-W., Harrison, D. H. T., and Moran, G. R. (2004) The structure of the ferrous form of (4-hydroxyphenyl)-pyruvate dioxygenase from *Streptomyces avermitilis* in complex with the therapeutic herbicide, NTBC, *Biochemistry 43*, 6370−6377.
36. Studier, F. W., and Moffatt, B. A. (1986) Use of bacteriophage T7 RNA polymerase to direct selective high-level expression of cloned genes, *J. Mol. Biol. 189*, 113−130.
37. Norris, S. R., Shen, X. H., and DellaPenna, D. (1998) Complementation of the Arabidopsis pds1 mutation with the gene encoding p-hydroxyphenylpyruvate dioxygenase, *Plant Physiol. 117*, 1317−1323.
38. Yang, C., Pflugrath, J. W., Camper, D. L., Foster, M. L., Pernich, D. J., and Walsh, T. A. (2004) Structural basis for herbicidal inhibitor selectivity revealed by comparison of crystal structures

of plant and mammalian 4-hydroxyphenylpyruvate dioxygenases, *Biochemistry 43*, 10414−10423.
39. Pace, N. C., Vajdos, F., Fee, L., Grimsley, G., and Gray, T. (1995) How to measure and predict the molar absorption coefficient of a protein, *Protein Sci. 4*, 2411−2423.
40. Patrie, S. M., Charlebois, J. P., Whipple, D., Kelleher, N. L., Hendrickson, C. L., Quinn, J. P., Marshall, A. G., and Mukhopadhyay, B. (2004) Construction of a hybrid quadrupole/Fourier transform ion cyclotron resonance mass spectrometer for versatile MS/MS above 10 kDa, *J. Am. Soc. Mass Spectrom. 15*, 1099−1108.
41. Senko, M. W., Canterbury, J. D., Guan, S., and Marshall, A. G. (1996) A high-performance modular data system for Fourier transform ion cyclotron resonance mass spectrometry, *Rapid Commun. Mass Spectrom. 10*, 1839−1844.
42. Grabski, A., Mehler, M., and Drott, D. (2003), *inNovations (Novagen)*, 1−6.
43. Lederer, B., and Boger, P. (2005) Recombinant p-hydroxyphenylpyruvate dioxygenase of high activity, *Z. Naturforsch., C: Biosci. 60*, 549−556.
44. Roche, P. A., Moorehead, T. J., and Hamilton, G. A. (1982) Purification and properties of hog liver 4-hydroxyphenylpyruvate dioxygenase, *Arch. Biochem. Biophys. 216*, 62−73.
45. Copik, A. J., Waterson, S., Swierczek, S. I., Bennett, B., and Holz, R. C. (2005) Both nucleophile and substrate bind to the catalytic Fe(II)-center in the type-II methionyl aminopeptidase from Pyrococcus furiosus, *Inorg. Chem. 44*, 1160−1162.
46. Narvaez, A. J., Kalman, L., LoBrutto, R., Allen, J. P., and Williams, J. C. (2002) Influence of the protein environment on the properties of a tyrosyl radical in reaction centers from *Rhodobacter sphaeroides*, *Biochemistry 41*, 15253−15258.
47. Elleingand, E., Gerez, C., Un, S., Knupling, M., Lu, G., Salem, J., Rubin, H., Sauge-Merle, S., Laulhere, J. P., and Fontecave, M. (1998) Reactivity studies of the tyrosyl radical in ribonucleotide reductase from *Mycobacterium tuberculosis* and *Arabidopsis thaliana*- -comparison with *Escherichia coli* and mouse, *Eur. J. Biochem. 258*, 485−490.
48. Svistunenko, D. A., Dunne, J., Fryer, M., Nicholls, P., Reeder, B. J., Wilson, M. T., Bigotti, M. G., Cutruzzola, F., and Cooper, C. E. (2002) Comparative study of tyrosine radicals in hemoglobin and myoglobins treated with hydrogen peroxide, *Biophys. J. 83*, 2845−2855.
49. Ryle, M. J., Liu, A., Muthukumaran, R. B., Ho, R. Y., Koehntop, K. D., McCracken, J., Que, L., Jr., and Hausinger, R. P. (2003) O2- and alpha-ketoglutarate-dependent tyrosyl radical formation in TauD, an alpha-keto acid-dependent non-heme iron dioxygenase, *Biochemistry 42*, 1854−1862.
50. Neidig, M. L., Decker, A., Kavana, M., Moran, G. R., and Solomon, E. I. (2005) Spectroscopic and computational studies of NTBC bound to the non-heme iron enzyme (4-hydroxyphenyl)-pyruvate dioxygenase: Active site contributions to drug inhibition, *Biochem. Biophys. Res. Commun. 338*, 206−214.
51. Hager, S. E., Gregerman, R. I., and Knox, W. E. (1957) p-Hydroxyphenylpyruvate oxidase of liver, *J. Biol. Chem. 225*, 935−947.
52. Lindblad, B., Lindstedt, G., and Lindstedt, S. (1970) The Mechanism of enzymic formation of homogentisate from p-hydroxyphenylpyruvate, *J. Am. Chem. Soc. 92*, 7446−7449.
53. Rundgren, M. (1982) Tritium isotope effects in the reaction catalyzed by 4- hydroxyphenylpyruvate dioxygenase from *Pseudomonas sp*. strain P. J. 874, *Biochim. Biophys. Acta 704*, 59−65.
54. Lindblad, B., Lindstedt, S., and Steen, G. (1977) On the enzymic defects in hereditary tyrosinemia, *Proc. Natl. Acad. Sci. U.S.A. 74*, 4641−4645.
55. Beltran-Valero de Bernabe, D., Jimenez, F. J., Aquaron, R., and Rodriguez de Cordoba, S. (1999) Analysis of alkaptonuria (AKU) mutations and polymorphisms reveals that the CCC sequence motif is a mutational hot spot in the homogentisate 1,2 dioxygenase gene (HGO), *Am. J. Hum. Genet. 64*, 1316−1322.
56. Fernandez-Canon, J. M., Granadino, B., Beltran-Valero de Bernabe, D., Renedo, M., Fernandez-Ruiz, E., Penalva, M. A., and Rodriguez de Cordoba, S. (1996) The molecular basis of alkaptonuria, *Nat. Genet. 14*, 19−24.
57. Garcia, I., Job, D., and Matringe, M. (2000) Inhibition of *p*-hydroxyphenylpyruvate dioxygenase by the diketonitrile of isoxaflutole: a case of half-site reactivity, *Biochemistry 39*, 7501−7507.
58. Fritze, I. M., Linden, L., Freigang, J., Auerbach, G., Huber, R., and Steinbacher, S. (2004) The crystal structures of *Zea mays* and *Arabidopsis* 4-hydroxyphenylpyruvate dioxygenase, *Plant Physiol. 134*, 1388−400.
59. Kindl, H. (1969) Biosynthesis and metabolism of hydroxyphenylacetic acids in higher plants, *Eur. J. Biochem. 7*, 340−347.
60. Olivera, E. R., Minambres, B., Garcia, B., Muniz, C., Moreno, M. A., Ferrandez, A., Diaz, E., Garcia, J. L., and Luengo, J. M. (1998) Molecular characterization of the phenylacetic acid catabolic pathway in *Pseudomonas putida* U: the phenylacetyl-CoA catabolon, *Proc. Natl. Acad. Sci. U.S.A. 95*, 6419−6424.
61. Knappskog, P. M., Eiken, H. G., Martinez, A., Flatmark, T., and Apold, J. (1995) The PKU mutation S349P causes complete loss of catalytic activity in the recombinant phenylalanine hydroxylase enzyme, *Hum. Genet. 95*, 171−173.
62. Armstrong, M. D., Shaw, K. N., and Robinson, K. S. (1955) Studies on phenylketonuria. II. The excretion of o-hydroxyphenylacetic acid in phenylketonuria, *J. Biol. Chem. 213*, 797−804.
63. Dyson, J. S., Beulke, S., Brown, C. D., and Lane, M. C. (2002) Adsorption and degradation of the weak acid mesotrione in soil and environmental fate implications, *J. Environ. Qual. 31*, 613−618.

BI052409C